Journal of Power Sources 254 (2014) 353–359

Contents lists available at ScienceDirect

Journal of Power Sources

journal homepage: www.elsevier.com/locate/jpowsour

Enhanced performance of lithium sulfur battery with polypyrrole warped mesoporous carbon/sulfur composite

Guoqiang Ma, Zhaoyin Wen*, Jun Jin, Yan Lu, Kun Rui, Xiangwei Wu, Meifen Wu, Jingchao Zhang

CAS Key Laboratory of Materials for Energy Conversion, Shanghai Institute of Ceramics, Chinese Academy of Sciences, Shanghai 200050, PR China

HIGHLIGHTS

- A novel approach for high-rate lithium sulfur batteries.
- 3D cubic mesoporous carbon CMK-8 was used as the matrix of the sulfur.
- A wrapping microstructure was designed and obtained with PPy as the coating layer of the CMK-8/S composite.
- This work makes much sense to the structure designing of novel sulfur-based materials.

GRAPHICAL ABSTRACT

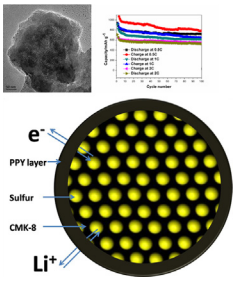

ARTICLE INFO

Article history:
Received 30 September 2013
Received in revised form
26 November 2013
Accepted 19 December 2013
Available online 27 December 2013

Keywords:
Lithium sulfur battery
Sulfur cathode
Cubic mesoporous carbon
Conductive polymer
Cycling performance

ABSTRACT

A sulfur cathode is designed with three-dimensional (3D) cubic mesoporous carbon CMK-8 as the matrix of sulfur, and polypyrrole (PPY) as the wrapping layer. CMK-8 provides perfect 3D conductive network. Furthermore, PPY is coated onto the surface of CMK-8/sulfur (CMK-8/S) composite to inhibit the migration of lithium polysulfide and offer better lithium ion conductive channels. The microstructure and electrochemical performance of the PPY@CMK-8/sulfur (PPY@CMK-8/S) cathode are investigated systematically. The results show that PPY layer with about 50 nm thickness is coated uniformly on the surface of CMK-8/S. The Li–S battery with PPY@CMK-8/S as cathode material presents a discharge capacity of 937.8 mAh g^{-1} at 20 cycles and is stabilized at about 860 mAh g^{-1} after 100 cycles at 0.2C.

1. Introduction

Li-ion battery is one of the most important rechargeable batteries in modern society. However, it still can't meet energy requirements for many applications, such as electric vehicle, large scale energy storage et al. [1,2]. The relatively low capacity of cathodes is one of the main obstacles achieving the high specific energy. As known, sulfur cathode has a theoretical capacity of 1675 mAh g^{-1} and a theoretical specific energy of 2600 Wh kg^{-1}, which are much higher than that of the commercialized $LiCoO_2$ system [3]. Therefore, in combination with the natural abundance, low cost and environmental friendliness of sulfur, the Li–S high

* Corresponding author. Shanghai Institute of Ceramics, Chinese Academy of Sciences, 1295 DingXi Road, Shanghai 200050, PR China. Tel.: +86 21 52411704; fax: +86 21 52413903.
E-mail address: zywen@mail.sic.ac.cn (Z. Wen).

0378-7753
http://dx.doi.org/10.1016/j.jpowsour.2013.12.085

energy density battery system becomes a promising candidate for the next generation power source.

Lithium sulfur (Li–S) battery has been studied for almost 50 years since Herbt and Ulam first introduced the concept of elemental sulfur as a positive electrode material in 1962. However, the spotlight hasn't returned to this battery system until there is a renewed interest in electric vehicles in recent years. The major impediments to the development of Li–S battery are low active material utilization rate, poor cycle life and low coulombic efficiency [4,5]. The insulating nature of sulfur and lithium sulfides decreases the utilization rate of active material. And the high solubility of lithium polysulfides generated during the electrochemical-reduction reaction process, results in severe capacity loss. The so called shuttle mechanism resulting from the migration of lithium polysulfides in the liquid electrolyte, even penetrating through the separator, followed by immediate reaction with metallic-lithium anode and the formation of Li_2S, is considered as the major reason for the low coulombic efficiency. Moreover, the gradually deposition and aggregation of insulating Li_2S on the cathode's surface results in a poor high-rate capacity and cycle stability.

To overcome these problems, sulfur embedding in the conductive carbon matrix has been adopted frequently. Various carbon materials such as active carbon [6], mesoporous carbon [7–10], carbon nanotubes [11,12], grapheme [13,14], microporous carbon [15,16], and porous hollow carbon [17,18] have been applied to achieve the purpose.

It was reported that with CMK-3, an ordered mesoporous carbon with high specific surface area and large pore volume, acting as the absorbent and matrix of sulfur, the Li–S battery exhibited reversible capacities up to 1350 mAh g^{-1} [8,10]. However, polysulfide can still dissolve in the electrolyte without any kinetic and chemical constraints, leading to a poor cycle performance. To inhibit the shuttle behaviors, conductive polymers such as PEDOT:PSS [19], PEO-PPO [20] and PANi [21] were adopted as coatings onto the surface of S/C composite. Since the good conduction feature of the conductive polymer, the coating layer affords the sulfur cathode low interfacial polarization, and hinders the polysulfides dissolution.

CMK-8 is a kind of 3-dimensional highly conductive mesoporous carbon, which has been widely used in supercapacitors [22] and catalytic [23,24]. However, there are few reports about the application of CMK-8 in the Li–S battery. Polypyrrole is another kind of conductive, whose dual conductive is beneficial to improve the rate ability [25]. Furthermore, the rich functional groups of PPY owe chemical trapping of polysulfides. In addition, the mechanical properties of PPY allows for better accommodation of volume expansion than pure carbon coatings [26]. Herein, the mesoporous carbon CMK-8 is prepared and acts as the matrix to load sulfur. PPy [25,27] is coated onto the surface of CMK-8/sulfur composite using a simple chemical oxidative polymerization method, then a wrapping micro-structure composite could be realized as shown in Fig. 1. In the obtained PPy@CMK-8/S composite, the sulfur nano-particles were penetrated into the channels of cubic mesoporous carbon CMK-8, and the CMK-8/S composite was wrapped with PPy. The 3D conductive networks and the coating layer for sulfur active material are favorable to improve the utilization rate of sulfur and coulombic efficiency, moreover to decrease the interfacial polarization.

2. Experimental

2.1. Preparation of PPY@CMK-8/S composite

The mesoporous carbon CMK-8 was prepared by the nanocasting process using sucrose as a precursor, mesoporous silica

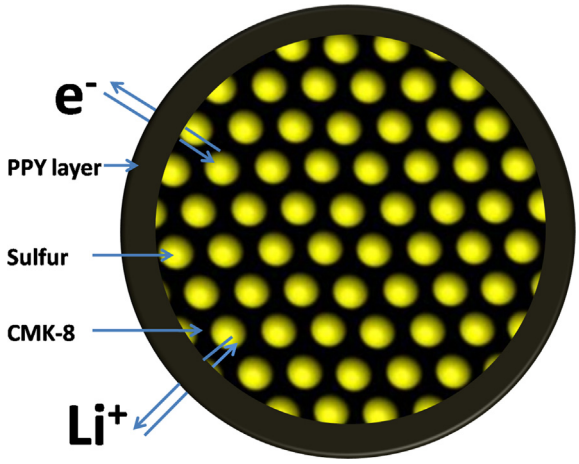

Fig. 1. The schematic diagram of the wrapping micro-structure composite.

KIT-6 as the hard template and sulfuric acid as the carbonization catalyst according to the literature [22,28]. The CMK-8/sulfur composite (CMK-8/S) was prepared by a melting-diffusion strategy with a mixture of sulfur and CMK-8 in the weight ratio of 3:1 and 3:2 respectively was sealed in a glass tube under vacuum followed by co-heating at 155 °C for 3 h and 300 °C for 2 h. The pitaya like PPY@CMK-8/sulfur composite (PPY@CMK-8/S) was prepared as follows: 0.4 g CMK-8/S (sulfur and CMK-8 in the weight ratio of 3:1) was dispersed in 200 ml deionized water by sonication for 30 min. Then, 0.1 g pyrrole was added into the solution and stirred for 30 min. After that, proper amount of $FeCl_3$ was added dropwise and stirred for 12 h, the chemical reaction was controlled under 2 °C. The product was washed and filtered until the filtrate was colorless. Finally, the products were dried under vacuum at 60 °C for 12 h. In order to obtain close sulfur contents in CMK-8/S and PPY@CMK-8/S composite, more content of sulfur in CMK-8/S composite is used to be wrapped with PPY.

2.2. Preparation of the sulfur cathode and coin-type cell

To prepare the cathode, the slurry was prepared by mixing 80 wt % PPY@CMK-8/S composite, 10 wt% acetylene black (AB), 5 wt% carboxy methyl cellulose (CMC), 5 wt% (styrene-butadiene rubber) SBR with deionized water was first prepared by ball milling. For comparison, the slurry of CMK-8/S composite (sulfur and CMK-8 in the weight ratio of 3:2) was prepared in the same way. The slurries were casted onto aluminum foil substrates. After the solvent was evaporated, the electrode was cut into discs with 14 mm in diameter and then dried at 60 °C under vacuum for 12 h. CR2025 type coin cells were assembled in a glove box with oxygen and water contents less than 1 ppm. A solution of 1 M LITFSI dissolved in DOL/DME/PYR_{14}TFSI (v/v/v, 2/2/1) was employed as the electrolyte. The cells contained Celgard 2400 as the separator and lithium foils as both the counter and reference electrodes.

2.3. Characterization

Thermogravimetry (TG) (NETZSCH 409 PC) was applied under N_2 atmosphere to determine the components of the composite. FTIR spectra were carried out on the Thermo Nicolet 7000-C Fourier Transform Spectrometer with ±2 cm^{-1} resolution between 4000 and 400 cm^{-1} using KBr disk method. Specific surface area was tested using the Brunauer–Emmett–Telley (BET) method on the Micromeritics Tristar 3000. SEM images were measured by field emission scanning electron microscope (FESEM JSM-6700) and

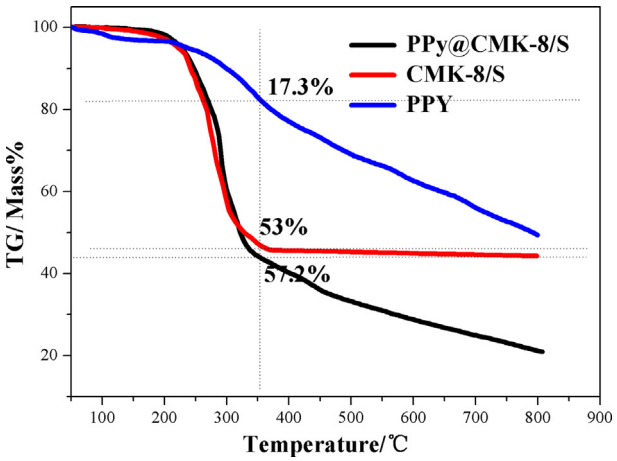

Fig. 2. TG profiles of PPY, PPy@CMK-8/S and CMK-8/S composite.

scanning electron microscope (Hitachi S-3400N). Transmission electron microscopy (TEM) images were measured on a JEOL JEM-2010 transmission electron microscope.

AC impedance measurement was carried out by a Frequency Response Analyzer (FRA) technique on an Autolab Electrochemical Workstation over the frequency range from 1 MHz to 10 MHz with the amplitude of 10 mV. Cyclic-voltammetry (CV) measurement was also conducted using the Autolab Electrochemical Workstation. The galvanostatic charge and discharge tests were conducted on a LAND CT2001A battery test system in a voltage range of 1.5–3.0 V (vs. Li/Li^+) at a current density of 0.1 mA cm^{-2}.

3. Results and discussion

3.1. Determination of components of the composites

The content of sulfur in the CMK-8/S and PPy@CMK-8/S composite are determined by TG analyses as we applied previously [29]. As seen in Fig. 2, the weight loss of PPY, CMK-8/S and PPY@CMK-8/S composite before 350 °C is 17.3%, 53% and 57.2% respectively, and there is 20% PPY in PPY@CMK-8/S composite. we considered sulfur was evaporated totally before 350 °C. So the sulfur content in PPY@CMK-8/S composite is calculated as follows:

$$20\% \times 17.3\ \text{wt\%} + X = 57.2\%,\ X = 53.74\%.$$

The sulfur content of CMK-8/S is close to that of PPY@CMK-8/S, so the enhanced electrochemical can only be attributed to the introduction of PPY.

3.2. FTIR analysis of the composite

The XRD patterns and FTRI spectrum of the different samples are showed in Fig. 3. As seen, the XRD pattern of CMK-8 is consistent with the previous result [24]. Usually, sulfur exists in a crystalline state with an orthorhombic structure. The XRD pattern of PPy@CMK-8/S composite is similar with that of CMK-8/S composite, however, the peak intensities of the sulfur in PPy@CMK-8/S is lower evidently than those of CMK-8/S composite. The bands at 3430 cm^{-1} and 1650 cm^{-1} are assigned respectively to the stretching and bending vibrations of the −OH groups of crystalline and adsorbed water molecules in CMK-8/S. In the spectrum of PPy@CMK-8/S composite, the peaks at 1545 cm^{-1} and 1458 cm^{-1} are attributed to the fundamental vibration of pyrrole ring, along with the =C−H in plane vibration at 1291 cm^{-1} and 1043 cm^{-1}, and the C−N stretching vibration at 1175 cm^{-1}, which is consistent with the results of Sun [30] and Liang [29]. The absorption intensity assigning to CMK-8/S composite in the spectra of PPy@CMK-8/S is weaker than that of CMK-8/S. Therefore, it is confirmed that PPy has been coated on the surface of CMK-8/S composite, which is similar to the existence of PPy on the surface of MWCNT [29].

3.3. Morphology and of the composites

The specific surface area and pore-distribution analyses of CMK-8 and CMK-8/S composite are conducted using N_2 adsorption and desorption experiments. As seen in Fig. 4, the BET surface area of CMK-8 is 1187 $m^2\ g^{-1}$, the mesopore volume is 1.36 $m^3\ g^{-1}$, and the average pore diameter is 5.05 nm. However, the surface area of CMK-8/S composite is only 1.47 $m^2\ g^{-1}$, and there is almost no pore in the CMK-8/S composite, indicating that the mesopores of CMK-8 are occupied by sulfur. Simultaneously, there is less than 55% sulfur in the CMK-8, whose volume is 0.61 cm^3 for 1 g CMK-8, and it is reported that the volume expansion of sulfur during the charge/discharge process reaches about 80% [31]. That is to say, the volume of the activity material after lithiation is about 1.098 cm^3 for 1 g CMK-8, which is still smaller than the pore volume in 1 g CMK-8. Therefore, there is still void space inner the CMK-8/S composite even after lithiation, which buffers the volume expansion of sulfur during the charge/discharge process, indicating a good cycling performance of the cell.

The TEM images for different samples are showed in Fig. 5. As seen, the CMK-8 exhibits a long-range-ordered meso-structure in the whole domain. As we know, the structure of CMK-8 is exactly an inverse replica of KIT-6, which consists of 3D cubic (Ia3d symmetry) mesoporous tubes [22]. Moreover, the carbon nanorods are interconnected by spacer, which is constituted by carbon that filled the

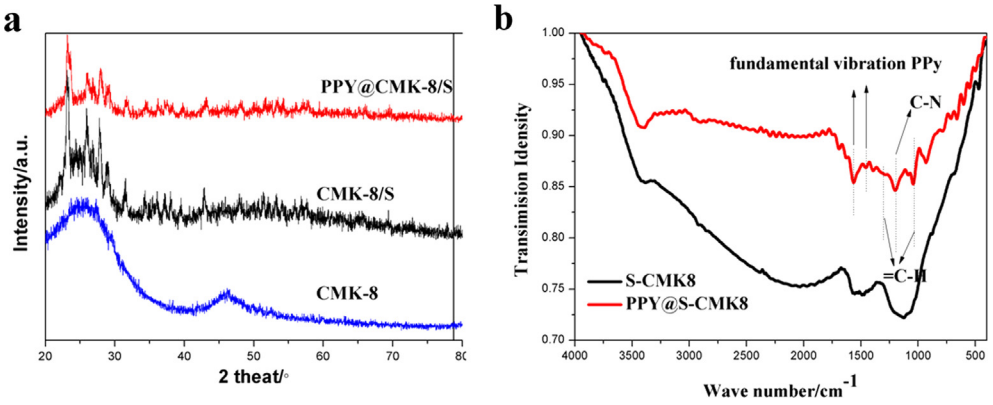

Fig. 3. XRD patterns of CMK-8, CMK-8/S and PPY@CMK-8/S (a), FTRA spectra of CMK-8/S and PPY@CMK-8/S (b).

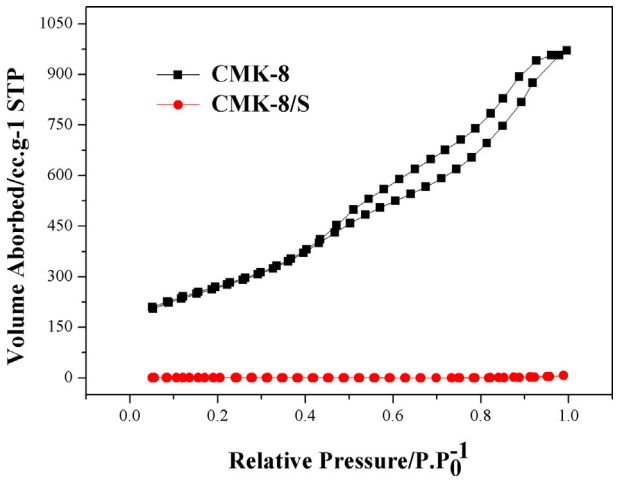

Fig. 4. N_2 adsorption/desorption isotherm of CMK-8 and CMK-8/S composite.

channel-interconnected micro-pores within the KIT-6 wall. Thus, the CMK-8 has an interpenetrating bi-continuous network of channels. After the sublimed sulfur penetrated into the channels of the CMK-8 by heating, the ordered pattern of the outside and inner channels of the mesoporous carbon turned into ambiguity, as shown in Fig. 5b. Comparison of the TEM images of the CMK-8 with the CMK-8/S composite accordingly confirms that sulfur is loaded in the channels of the OMCs. Meanwhile, the PPY coating layer on the CMK-8/S composite surface can be observed clearly in Fig. 5c, whose thickness is about 50 nm. Consequently, a wrapped structure is obtained with PPY as the coating layer and CMK-8 as matrix of sulfur. Such a 3D conductive structure can further enhance the conductivity by reducing the contact resistance among the particles. Besides, the coating layer can effectively prevent the dissolution and migration of lithium polysulfide in the liquid electrolyte. As shown in Fig. 5d, the wrapping structure is stable even after 40 charge/discharge cycles, demonstrating the volume expansion is buffered by the large pore volume of CMK-8, indicating a good cycling performance for Li–S battery.

3.4. Cycling voltammogram and charge/discharge profiles

Cyclic voltammograms (CVs) of the CMK-8/S sample and the PPy@CMK-8/S sample are shown in Fig. 6a and b. As seen, there are two cathodic peaks respectively for the two samples, owing to the two-step reduction of sulfur in the presence of Li-ion. Moreover, the cathodic peaks potential of the first cycle are lower, while the anodic peak potential is higher than that of the following cycles, indicating that there is electrochemical activation in both samples, while the PPy@CMK-8/S sample could get electrochemical activation more easily. Correspondingly, there are two discharge potential plateaus in the initial charge/discharge potential profiles of the two samples as Fig. 7 indicated. The two discharge potential plateaus of the PPy@CMK-8/S sample are higher than that of the CMK-8/S sample, and the charge potential plateau of PPy@CMK-8/S cathode is lower than that of the CMK-8/S cathode, further proving lower polarization for the PPy@CMK-8/S composite.

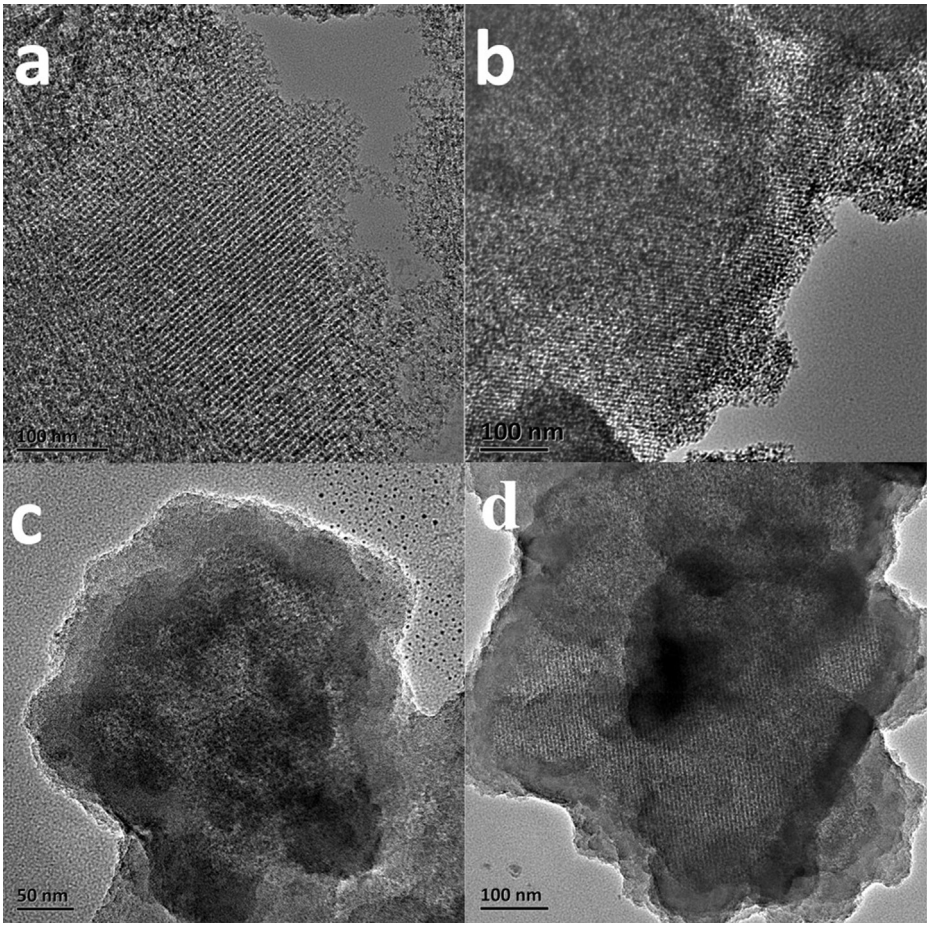

Fig. 5. TEM images of CMK-8 (a), CMK-8/S (b), PPy@CMK-8/S composite (c) and PPy@CMK-8/S (d) cathode after 40 cycles.

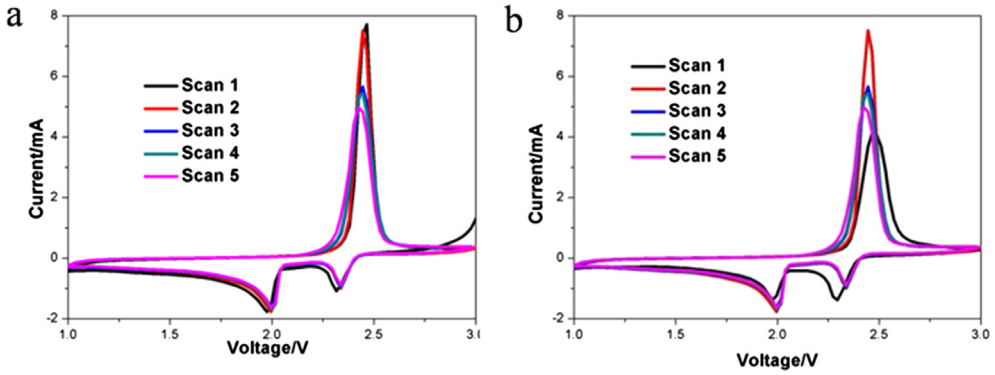

Fig. 6. Cyclic voltammogram profiles of PPy@CMK-8/S cathode (a) and CMK-8/S cathode (b).

The cycling performances and the coulombic efficiencies of both the PPy@CMK-8/S and CMK-8/S composite at 0.2C (1C = 1675 mAh g^{-1}) are shown in Fig. 8. As seen, initial discharge capacity of the CMK-8/S cathode is 970 mAh g^{-1}, while the PPY@CMK-8/S sample delivers 1099 mAh g^{-1}, which is about 13.2% higher than that of uncoated CMK-8/S. The CMK-8/S sample shows continuous discharge capacity degradation and columbic efficiency fading. A specific discharge capacity of is only 577 mAh g^{-1} at 100th cycle with the coulombic efficiency of as low as 81%. It is likely that although lithium polysulfides can be trapped in the pores of mesoporous carbon to some extent, their dissolution and diffusion of lithium polysulfides in the electrolyte are obvious. In contrast, the PPy@CMK-8/S cathode shows certain decay at the beginning, but a nearly constant discharge capacity stabilizes at around 880 mAh g^{-1} with 20th–100th cycles. An average decay rate of only 0.103% per cycle is obtained during the 80 cycles. It is proposed that lithium polysulfides are trapped inside the inner surface of PPy coating layer. While the PPy@CMK-8/S displays lower initial columbic efficiency than the uncoated cathode for the first cycles because of the side effect, it continuously increase within the whole cycling span and reaches a value close to 92.2% at the 100th cycle, suggesting an effective inhibition effect of the PPy layer for the dissolution and diffusion of the lithium polysulfides.

3.5. Rate performances

The rate performances of the PPy@CMK-8/S and CMK-8/S composites are evaluated. Fig. 9a shows the cycling stability of the both composite by a stepping mode. As seen, an initial discharge specific capacity of 1171 mAh g^{-1} at 0.1C for PPy@CMK-8/S is achieved. And the maximum capacities of the cathode at 2C and 4C are 562 mAh g^{-1} and 451 mAh g^{-1}, reaching 48.0% and 38.5% of that at 0.1C, respectively. However, the maximum capacities of CMK-8/S composite are 346 mAh g^{-1} at 2C and 273 mAh g^{-1} at 4C, only 35.1% and 27.6% of the maximum capacity at 0.1C, demonstrating much better rate performance of PPy@CMK-8/S composite than that of CMK-8/S composite. Besides, Fig. 9b shows longer cycling performances of PPy@CMK-8/S at different rates. The initial discharge capacities of 949 mAh g^{-1}, 912 mAh g^{-1} and 643 mAh g^{-1} are shown for the PPy@CMK-8/S composite at 0.5C, 1C and 2C respectively. The exceptional high-rate capability in the initial cycle is mainly attributed to the synergistic effect of the good conductive CMK-8 as the matrix and the conductive PPy [25] as coating layer on the surface. The cycling stability is enhanced significantly at higher rates, giving rise to the remaining of 717, 620 and 526 mAh g^{-1} at 0.5C, 1C and 2C respectively even after 100 cycles, owing to the stable core–shell structure comprised of PPy coating layer and CMK-8/S composite.

3.6. Electrochemical impedance spectra

Actually, the rate capability and cycle stability are mainly related to the interfacial charge transfer process and lithium ion diffusion in the cell, due to the inescapable aggregation of insulated Li_2S on the cathode surface during circulation. To get further insight into the electrochemical reaction process, electrochemical impedance spectra (EIS) of the PPy@CMK-8/S at the fully charged states after different cycles are measured and presented in Fig. 10. As seen, the

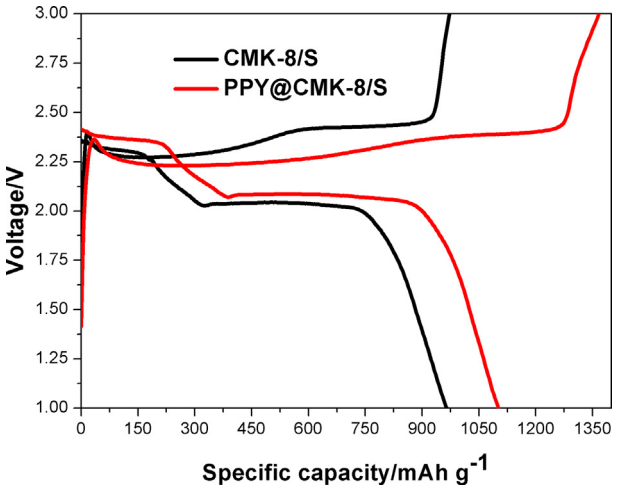

Fig. 7. Initial charge/discharge potential profiles of CMK-8/S and PPy@CMK-8/S composite.

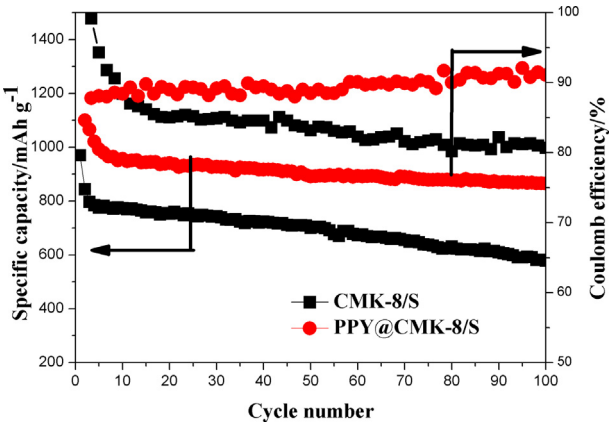

Fig. 8. Cycling performance and coulombic efficiency of the CMK-8/S composite and the PPy@CMK-8/S composite.

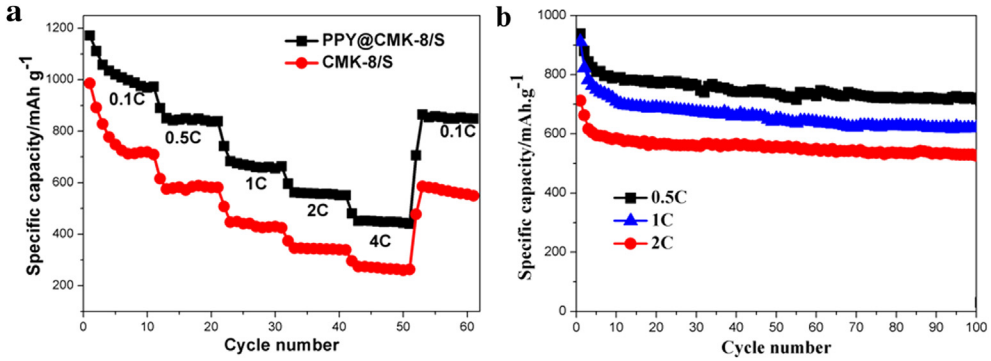

Fig. 9. Cycling and rate performance of the PPy@CMK-8/S and CMK-8/S (a), cycling performance of PPy@CMK-8/S at different rates (b).

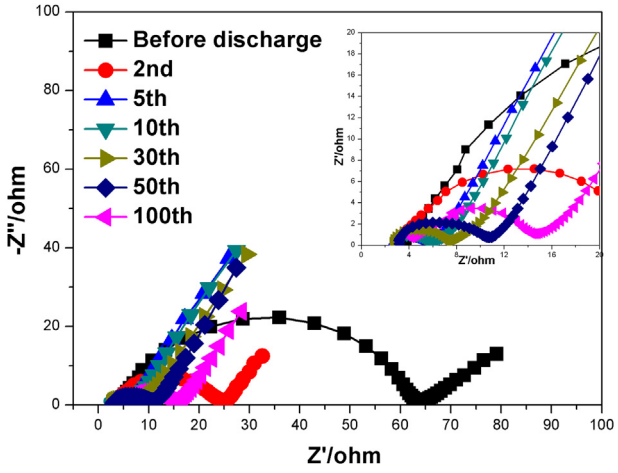

Fig. 10. EIS analysis of the PPy@CMK-8/S composite at different cycles after fully charged.

impedance plots are composed of a semicircle in the high frequency domain corresponding to the charge transfer impedance and interfacial impedance, and a sloping straight line in the low frequency domain corresponding to the Warburg impedance [21]. The impedance of the PPy@CMK-8/S sample decreases dramatically to the lowest value (5.6 Ω) after the fifth cycle from 64 Ω before discharging. Then the resistance value rises slightly to 12 Ω after 70th cycle, indicating that electrochemical activation occurs in the first several cycles, and the depositing and aggregating process on the surface of electrode are not serious in the following cycles for PPy@CMK-8/S sample. The favorable performance obtained with PPy@CMK-8/S electrodes demonstrates that PPy coating is an effective method to improve the electrochemical performance of Li–S batteries.

4. Conclusion

In summary, PPy@CMK-8/S cathode was obtained with cubic mesoporous CMK-8 to load sulfur and PPy as the coating layer. In particular, a stable charge/discharge capability was obtained for the PPy@CMK-8/S composite with 53.7 wt% S. The maximum discharge specific capacity reached 1099 mAh g^{-1} and still retained 860 mAh g^{-1} after 100 cycles at 0.2C. Moreover, the maximum discharge specific capacity retained at 620 mAh g^{-1} after 100 cycles at 1C. The enhanced performance is attributed to the synergistic effect of the three reasons as follows. Firstly, as the matrix of sulfur, the 3D conductive networks of CMK-8 enhance the conductivity of the cathode. Secondly, the conductive polymer coating layer inhibits the lithium polysulfides from dissolution and migration in the electrolyte, which suppress the shuttle mechanism significantly. The dual conductive PPy is also beneficial for the enhanced conductivity of the cathode, leading to the reduced polarization of the cathode. Thirdly, the volume expansion during charge/discharge process is buffered by the void space inner the CMK-8/S composite.

Acknowledgments

This work was financially supported by NSFC Project No.51373195; research projects from the Science and Technology Commission of Shanghai Municipality no. 08DZ2210900.

References

[1] A.S. Arico, P. Bruce, B. Scrosati, J.M. Tarascon, W. Van Schalkwijk, Nat. Mater. 4 (2005) 366–377.
[2] B. Kang, G. Ceder, Nature 458 (2009) 190–193.
[3] J. Shim, K.A. Striebel, E.J. Cairns, J. Electrochem. Soc. 149 (2002) A1321–A1325.
[4] Y.F. Arumugam Manthiram, Yu-Sheng Su, Acc. Chem. Res. 46 (2013) 1125–1134.
[5] S.E.A.L.F. Nazar, Acc. Chem. Res. 46 (2013) 1135–1143.
[6] J.Y.J.L. Wang, J.Y. Xie, N.X. Xu, Y. Li, Electrochem. Commun. 4 (2002) 499–502.
[7] S.-R. Chen, Y.-P. Zhai, G.-L. Xu, Y.-X. Jiang, D.-Y. Zhao, J.-T. Li, L. Huang, S.-G. Sun, Electrochim. Acta 56 (2011) 9549–9555.
[8] X.L. Ji, K.T. Lee, L.F. Nazar, Nat. Mater. 8 (2009) 500–506.
[9] H. Li, H.a. Xi, S. Zhu, Z. Wen, R. Wang, Microporous Mesoporous Mater. 96 (2006) 357–362.
[10] X.L. Ji, S. Evers, K.T. Lee, L.F. Nazar, Chem. Commun. 46 (2010) 1658–1660.
[11] C. Jia-jia, J. Xin, S. Qiu-jie, W. Chong, Z. Qian, Z. Ming-sen, D. Quan-feng, Electrochim. Acta 55 (2010) 8062–8066.
[12] M. Hagen, S. Dörfler, P. Fanz, T. Berger, R. Speck, J. Tübke, H. Althues, M.J. Hoffmann, C. Scherr, S. Kaskel, J. Power Sources 224 (2013) 260–268.
[13] F. Zhang, Y. Dong, Y. Huang, G. Huang, X. Zhang, L. Wang, J. Phys. Conf. Series 339 (2012) 012003.
[14] L. Yin, J. Wang, F. Lin, J. Yang, Y. Nuli, Energy Environ. Sci. 5 (2012) 6966–6972.
[15] B. Zhang, X. Qin, G.R. Li, X.P. Gao, Energy Environ. Sci. 3 (2010) 1531–1537.
[16] S. Xin, L. Gu, N.H. Zhao, Y.X. Yin, L.J. Zhou, Y.G. Guo, L.J. Wan, J. Am. Chem. Soc. 134 (2012) 18510–18513.
[17] N. Jayaprakash, J. Shen, S.S. Moganty, A. Corona, L.A. Archer, Angew. Chem. Int. Ed. 50 (2011) 5904–5908.
[18] K. Tang, R.J. White, X. Mu, M.-M. Titirici, P.A. van Aken, J. Maier, Chemsuschem 5 (2012) 400–403.
[19] Y. Yang, G.H. Yu, J.J. Cha, H. Wu, M. Vosgueritchian, Y. Yao, Z.A. Bao, Y. Cui, ACS Nano 5 (2011) 9187–9193.
[20] Y. Fu, Y.-S. Su, A. Manthiram, ACS Appl. Mater. Interfaces 4 (2012) 6046–6052.
[21] G.-C. Li, G.-R. Li, S.-H. Ye, X.-P. Gao, Adv. Energy. Mater. 2 (2012) 1238–1245.
[22] J.-W. Lang, X.-B. Yan, X.-Y. Yuan, J. Yang, Q.-J. Xue, J. Power Sources 196 (2011) 10472–10478.
[23] M. Lezanska, J. Wloch, G. Szymański, I. Szpakowska, J. Kornatowski, Catal. Today 150 (2010) 77–83.
[24] B. Li, X.H. Li, Y. Ding, P. Wu, Catal. Lett. 142 (2012) 1033–1039.

[25] Y. Cui, Z. Wen, Y. Lu, M. Wu, X. Liang, J. Jin, J. Power Sources 244 (2013) 614–619.
[26] Y. Yang, G. Zheng, Y. Cui, Chem. Soc. Rev. 42 (2013) 3018–3032.
[27] Y. Cui, Z. Wen, X. Liang, Y. Lu, J. Jin, M. Wu, X. Wu, Energy Environ. Sci. 5 (2012) 7893–7897.
[28] K.P. Gierszal, M. Jaroniec, T.W. Kim, J. Kim, R. Ryoo, New J. Chem 32 (2008) 981–993.
[29] X. Liang, Y. Liu, Z. Wen, L. Huang, X. Wang, H. Zhang, J. Power Sources 196 (2011) 6951–6955.
[30] M.M. Sun, S.C. Zhang, T. Jiang, L. Zhang, J.H. Yu, Electrochem. Commun. 10 (2008) 1819–1822.
[31] Z. Wei Seh, W. Li, J.J. Cha, G. Zheng, Y. Yang, M.T. McDowell, P.-C. Hsu, Y. Cui, Nat. Commun. 4 (2013) 1331–1336.